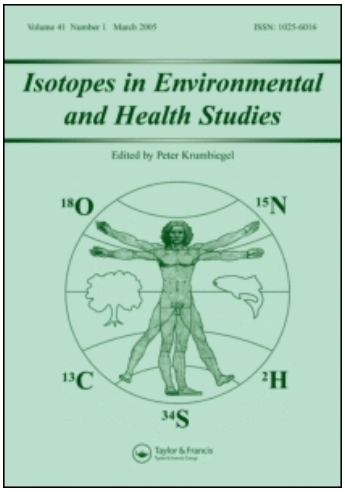

Isotopes in Environmental and Health Studies
Publication details, including instructions for authors and subscription information:
http://www.informaworld.com/smpp/title~content=t713643233

Nitrogen isotopes determination in natural gas: analytical method and first results on magmatic, hydrothermal and soil gas samples

Fausto Grassa[a]; Giorgio Capasso[a]; Ygor Oliveri[a]; Aldo Sollami[a]; Paula Carreira[b]; M. Rosário Carvalho[c]; José M. Marques[d]; João C. Nunes[e]
[a] Istituto Nazionale di Geofísica e Vulcanologia, Palermo, Italy [b] Instituto Tecnológico e Nuclear, Sacavém, Portugal [c] Faculdade de Ciências de Lisboa, Departamento de Geologia, CeGUL, Lisboa, Portugal [d] Instituto Superior Técnico, Lisboa, Portugal [e] Department of Geosciences, University of the Azores, Sao Miguel, Azores, Portugal

Online publication date: 23 June 2010

To cite this Article Grassa, Fausto , Capasso, Giorgio , Oliveri, Ygor , Sollami, Aldo , Carreira, Paula , Rosário Carvalho, M. , Marques, José M. and Nunes, João C.(2010) 'Nitrogen isotopes determination in natural gas: analytical method and first results on magmatic, hydrothermal and soil gas samples', Isotopes in Environmental and Health Studies, 46: 2, 141 — 155
To link to this Article: DOI: 10.1080/10256016.2010.491914
URL: http://dx.doi.org/10.1080/10256016.2010.491914

Isotopes in Environmental and Health Studies
Vol. 46, No. 2, June 2010, 141–155

Taylor & Francis
Taylor & Francis Group

Nitrogen isotopes determination in natural gas: analytical method and first results on magmatic, hydrothermal and soil gas samples†

Fausto Grassa[a], Giorgio Capasso[a]*, Ygor Oliveri[a], Aldo Sollami[a], Paula Carreira[b], M. Rosário Carvalho[c], José M. Marques[d] and João C. Nunes[e]

[a]*Istituto Nazionale di Geofísica e Vulcanologia, Sezione di Palermo, Palermo, Italy;* [b]*Instituto Tecnológico e Nuclear, Sacavém, Portugal;* [c]*Faculdade de Ciências de Lisboa, Departamento de Geologia, CeGUL, Lisboa, Portugal;* [d]*Instituto Superior Técnico, Lisboa, Portugal;* [e]*Department of Geosciences, University of the Azores, Sao Miguel, Azores, Portugal*

(*Received 18 December 2009; final version received 25 April 2010*)

A continuous-flow GC/IRMS technique has been developed to analyse δ^{15}N values for molecular nitrogen in gas samples. This method provides reliable results with accuracy better than 0.15 ‰ and reproducibility (1σ) within $\pm$0.1 ‰ for volumes of N_2 between 1.35 (about 56 nmol) and 48.9 μL (about 2 μmol).

The method was tested on magmatic and hydrothermal gases as well as on natural gas samples collected from various sites. Since the analysis of nitrogen isotope composition may be prone to atmospheric contamination mainly in samples with low N_2 concentration, we set the instrument to determine also N_2 and ^{36}Ar contents in a single run. In fact, based on the simultaneously determined $N_2/^{36}$Ar ratios and assuming that ^{36}Ar content in crustal and mantle-derived fluids is negligible with respect to ^{36}Ar concentration in the atmosphere, for each sample, the degree of atmospheric contamination can be accurately evaluated. Therefore, the measured δ^{15}N values can be properly corrected for air contamination.

Keywords: Argon-36; isotope measurement and technique; nitrogen-15; online measurements; volcanic and hydrothermal gas

1. Introduction

In the last decade, nitrogen molecular abundance and isotope ratios were discovered to be geochemical tracers of volatiles' source [1–4]. δ^{15}N values in gases emitted from fumaroles and hot springs in arc volcanic systems were used to better understand the nitrogen cycle in the subduction zones [5–8]. Moreover, in combination with noble gases and/or carbon isotope ratios, the δ^{15}N values provide useful data to constrain magma source, contamination processes as well as the source of nitrogen in natural gases [9–13].

However, the determination of the nitrogen isotope composition is strongly subjected to contamination by an atmospheric (air or air saturated water (ASW)) component. Therefore, the measured

*Corresponding author. Email: g.capasso@pa.ingv.it
†Contribution to the 8th Symposium on Applied Isotope Geochemistry (AIG) (30 August–4 September 2009, La Malbaie, Quebec, Canada).

ISSN 1025-6016 print/ISSN 1477-2639 online

DOI: 10.1080/10256016.2010.491914
http://www.informaworld.com

$\delta^{15}N_{N2}$ values have to be corrected for atmospheric contamination. There are many criteria that can be used to identify samples affected by atmospheric contribution. The most commonly used criterion is to take into account the oxygen contents and the N_2/O_2 molar ratios. However, oxygen may be involved in the redox processes and therefore, the N_2/O_2 molar ratios could be not representative of the effective atmospheric contribution. The N_2/Ar ratios are also used to monitor contamination by air and/or ASW, by assuming that Ar content in gas emissions is predominantly air-derived. However, production of radiogenic ^{40}Ar leads to ^{40}Ar/^{36}Ar ratios in air-free mantle-derived fluids (up to 21.500 in OIBs [14] and up to 42.000 in MORBs [15]) much higher than air/ASW (^{40}Ar/^{36}Ar = 295.5 [16]). Therefore, the use of N_2/Ar ratios in gas samples having ^{40}Ar/^{36}Ar ratios higher than air/ASW tends to over-estimate the degree of atmospheric contamination.

The more accurate methods to identify and to evaluate atmospheric contribution in gas samples are based on the $N_2/^{20}$Ne or the $N_2/^{36}$Ar ratios. These corrections are made on the assumption that ^{20}Ne and ^{36}Ar contents in mantle- and crustal-derived fluids are negligible with respect to those of atmospheric origin [17].

However, in order to determine both nitrogen isotopes and noble gas abundances, many of the traditional experimental methods (GC techniques, quadrupole and dual inlet mass spectrometer measurements) generally require different aliquots of gases.

More recently, new high-sensitivity multi-collector mass spectrometers were designed and specifically modified to simultaneously perform isotopic and elemental abundance measurements.

These instruments are very expansive and are generally used for analyses of micro-volume of gas extracted from fluid inclusions in minerals [9,11,12].

In this paper, a new simple analytical technique to simultaneously determine $\delta^{15}N_{N2}$ values, N_2 and ^{36}Ar contents in a single run is described and evaluated. This method, based on continuous-flow IRMS measurements, also allows accurate quantification of air contamination.

2. Method

2.1. *Technical set up*

The analytical instrument consists of a Thermo Delta Plus XP stable isotopes ratio mass spectrometer coupled with a Thermo TRACE Gas Chromatograph and a Thermo GC/C III interface.

The TRACE GC was equipped with an Rt®-Msieve 5A PLOT column (30 m × 0.32 mm OD), a molecular sieve column capable of separating efficiently Ar/O_2, N_2/CO and permanent gases. At the end of the column, an automated valves system (Backflush) and a NAFION™ water trap avoid that other gases (e.g. carbon monoxide having m/z 28 and water) interfere with IRMS measurements.

Thermo Delta^{Plus} XP IRMS is equipped with five universal collectors and configured to perform isotope analyses of H_2, CO_2, and N_2. Its fast mass switching magnet allows the measurement of consecutively multiple gases isotopes within the same run.

GC and IRMS are interfaced by means of a GC/C III device providing that gas eluting from GC as well as the reference gas from an external cylinder are transferred to IRMS. Oxidation and reduction reactors are kept at ambient temperature.

2.2. *Inlet system*

The inlet system consists of a 50 μl stainless steel loop connected to a two-position six-port Valco® valve (Figure 1). The samples, contained in glass flasks, are transferred to the injector

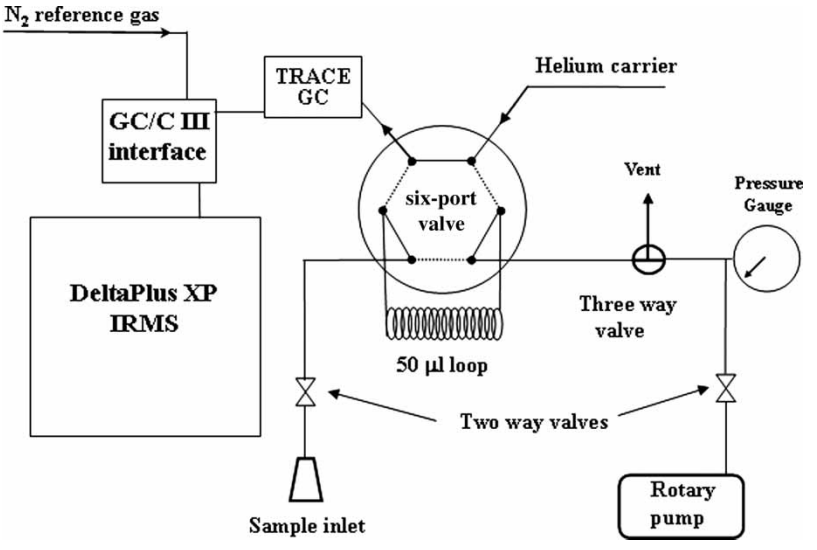

Figure 1. Schematics of the analytical instrument.

by means of stainless steel 1/16″ O.D. tubing. Prior to sample introduction, the inlet system was evacuated to about 10^{-2} kPa by an Edward RV3 rotary vane pump. An EBRO pressure gauge was used to measure the pressure inside the tubing. Once the vacuum had been reached, the sample was manually loaded in the loop with the valve in the 'load' position. After an equilibration time of 30 seconds, the valve was switched in the 'inject' position directing the sample to the injector (split/splitless type with split ratio of 10) and subsequently to the column. For low-concentration gas, a direct on-column injection can be used instead.

2.3. *Running the method*

By using helium (5.6) as a carrier gas at a constant flow of 1.3 cc/min and following an isothermal path at 50 °C, the elution times for ^{36}Ar and N_2 are about 300 and 370 s, respectively.

At the start, the IRMS is set on m/z 36 until the peak of Argon is resolved. At 325 s, the IRMS automatically jumps to m/z 28 and m/z 29 to detect nitrogen. Finally, at least four reference gas pulses of known isotope ratios are measured, thus allowing us to determine the $\delta^{15}N$ values. In Figure 2, a spectrum for an injection of air sample at atmospheric pressure is reported. Run-time analyses for elemental (^{36}Ar and N_2) composition and $^{15}N/^{14}N$ isotope ratio determination takes approximately 10 min.

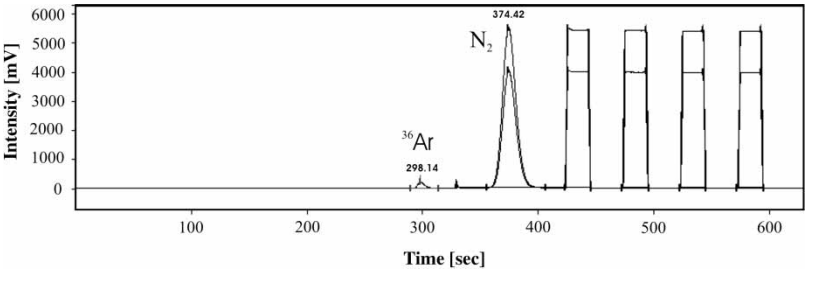

Figure 2. Spectrum for an injection of air sample at atmospheric pressure. Elution times for ^{36}Ar and N_2 are about 300 s and 370 s respectively. Total run time analyses takes approximately 10 minutes.

Quantitative detection limits for ^{36}Ar and N_2 were determined by running a sequence of calibrated air samples, injected at decreasing pressure levels. Air samples used as internal standards were collected outdoors and subsequently analysed for N_2 and ^{36}Ar contents using a Hewlett-Packard Clarus 500 GC equipped with a HWD detector and a GV Instruments ARGUS mass spectrometer, respectively.

The accuracy and the precision on nitrogen isotope measurements were tested on BIT gas, an in-house pure nitrogen gas (6.0) with $\delta^{15}N$ values of -1.4 ‰. The nitrogen isotope value of the N_2 reference gas cylinder was calibrated daily by air samples with $\delta^{15}N$ values of 0 ‰. The $\delta^{15}N$ values of both BIT (pure N_2) and calibrated air samples were determined at external laboratories (1σ better than 0.15 ‰). Finally, to the test the efficacy of GC separation and to evaluate the effects of possible interfering masses, three internal standard gases were prepared. These mixtures consist of BIT (99.5 %) and CO (0.5 %), BIT (85 %) and CO_2 (15 %), and BIT (99 %) CO (0.5 %) and CH_4 (0.5 %), respectively.

3. Determination of N_2 and ^{36}Ar concentration: calibration, reproducibility and detection limits

Five-point calibration curves were constructed by analysing three replicate air samples ($N_2 =$ 78 % and $^{36}Ar = 31.6$ ppm) at five pressure levels (from 14.1 to 126.6 kPa). By using a 50 µl loop, this pressure range is equivalent to a volumetric sample range of 5.4–49.0 µl (i.e. 0.24–2.18 µmol) of nitrogen and 0.22–1.98 nl (i.e. 10–88 pmol) of ^{36}Ar (Table 1). For each of the analyte (N_2 and ^{36}Ar), the respective calibration curve was produced by plotting the average peak area obtained from GC-IRMS measurements against the volume of the injected analyte. The selected ions used were m/z 28 for nitrogen and m/z 36 for ^{36}Ar. The relative standard deviation (RSD) of the peak area measured at the selected five pressure levels are less than 0.7 % and 1.2 % for m/z 28 and for m/z 36, respectively.

Two examples of calibration curves obtained during a single day of measurements are reported in Figure 3. For both N_2 and ^{36}Ar, a very good correlation ($R^2 > 0.9998$) exists between volume

Table 1. Results of the five-point calibration curves built by analysing three replicate air samples ($N_2 = 78$ % and $^{36}Ar = 31.6$ ppm) at five pressure levels.

Injection pressure (kPa)	Vol. ^{36}Ar (μl)	Vol. N_2 (μl)	Injected Volume (μl)	Area peak m/z 36	^{36}Ar RSD%	Area peak m/z 28	N_2 RSD%	$\delta^{15}N_{N2}$
126.6	2.0E-03	49.0	62.7	2.86		132.54		0.10
126.5	2.0E-03	48.9	62.7	2.84		131.65		−0.03
126.1	2.0E-03	48.9	62.7	2.81	0.86	130.98	0.60	0.08
100.9	1.6E-03	39.0	50.0	2.27		105.60		0.06
100.9	1.6E-03	39.0	50.0	2.29		104.60		−0.05
100.3	1.6E-03	39.0	50.0	2.27	0.52	105.10	0.47	−0.09
73.9	1.1E-03	28.1	36.0	1.62		74.79		−0.10
72.5	1.1E-03	28.0	35.9	1.65		75.12		−0.08
71.8	1.1E-03	27.8	35.6	1.61	1.20	74.16	0.65	0.03
53.0	8.2E-04	20.2	26.0	1.16		53.19		0.10
52.3	8.2E-04	20.2	25.9	1.19		53.58		0.03
52.1	8.2E-04	20.1	25.8	1.17	1.07	53.65	0.47	−0.06
14.4	2.2E-04	5.5	7.1	0.31		13.74		0.03
14.3	2.2E-04	5.5	7.1	0.31		13.72		−0.02
14.1	2.2E-04	5.4	7.0	0.31	0.99	13.85	0.50	−0.02

Notes: Injected volume = Volume of loop $\times P_{inj}/P_{atm}$; Area peak is reported in volts ×s; RDS% = Relative standard deviation for N_2 and ^{36}Ar area peak, computed at each pressure level.

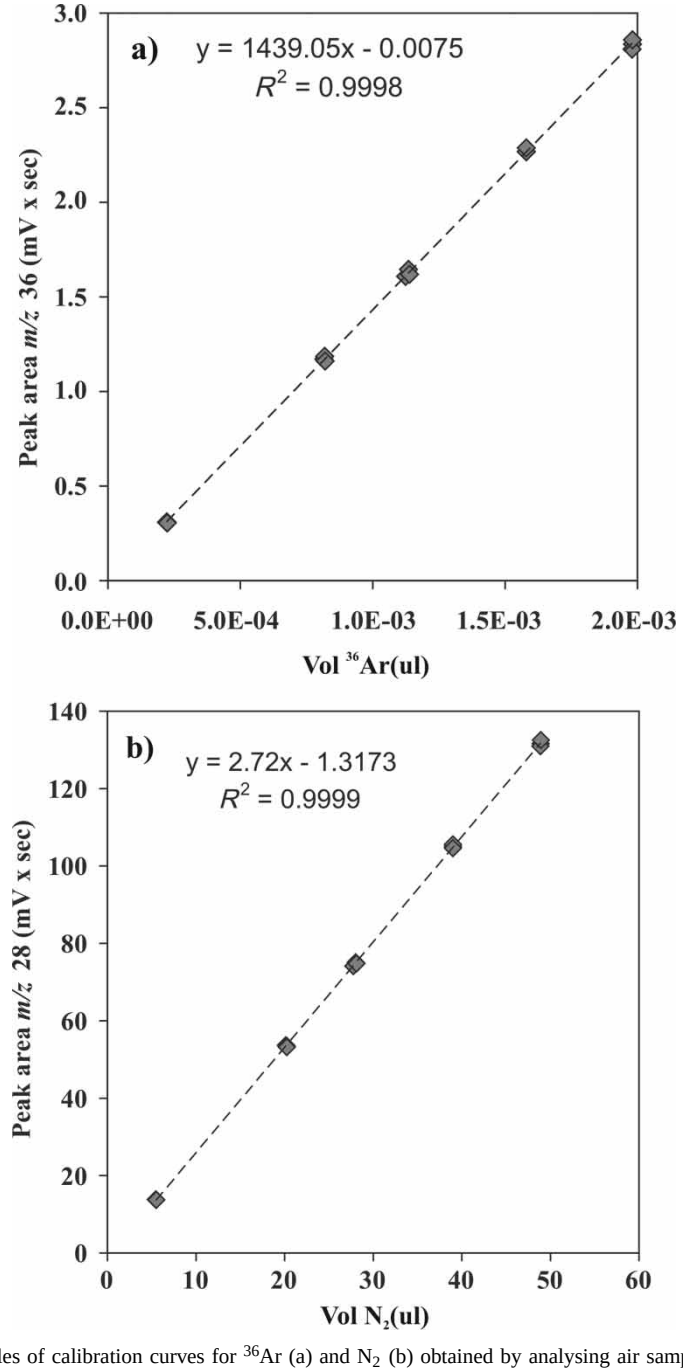

Figure 3. Examples of calibration curves for ^{36}Ar (a) and N_2 (b) obtained by analysing air samples at five pressure levels.

of injected gas and the average peak area of the analyte, thus highlighting a good linearity in the selected pressure range.

The results for all the air samples ($n = 40$) run over a nine-month period are also reported (Figures 4a and b). It can be seen that calibration curves obtained over this period show negligible differences in the slope of the linear regression with respect to those constructed daily.

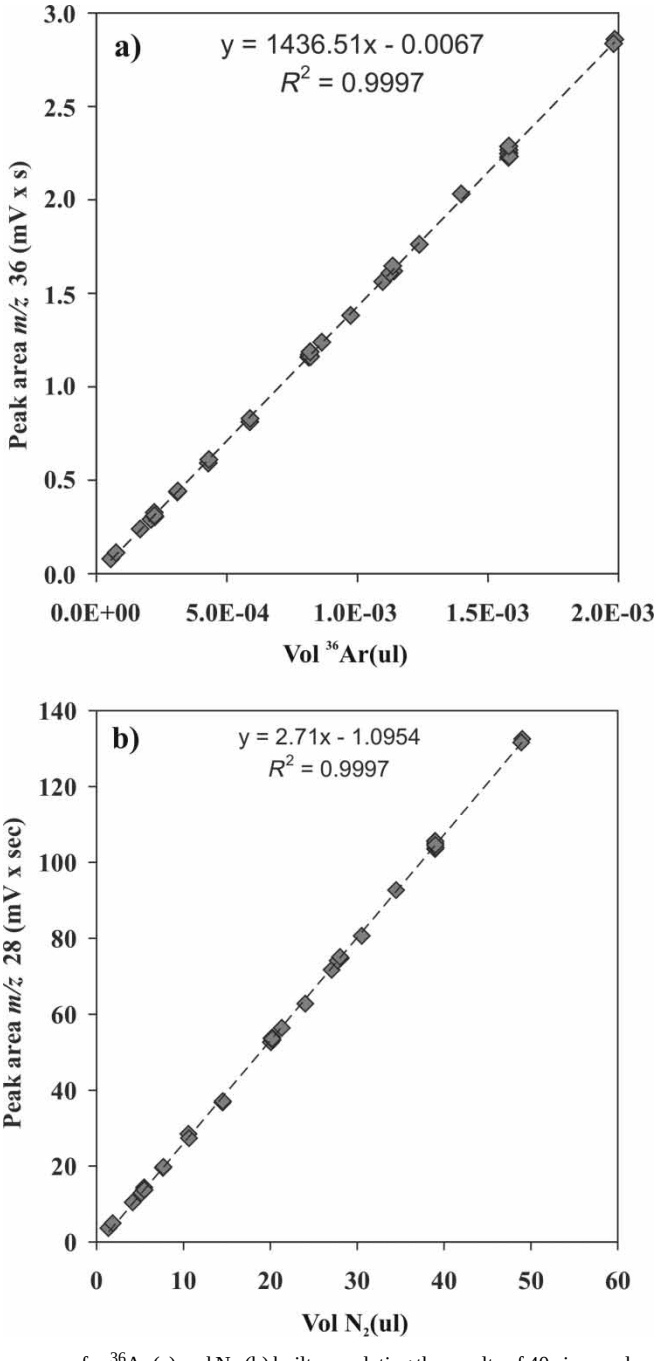

Figure 4. Calibration curves for ^{36}Ar (a) and N_2 (b) built cumulating the results of 40 air samples run over a nine-month period.

To define the lower limits of detection, air samples were injected at decreasing pressure levels until the linearity was maintained and the signal-to-noise ratio for m/z 36 was greater than 3:1. It can be seen that until the pressure decreases to 3.5 kPa, the volume of injected gas is still strongly correlated ($r^2 > 0.9997$) with the peak area for both m/z 28 (N_2 in Figure 4b) and m/z 36 (^{36}Ar

Table 2. δ^{15}N values obtained from injections of pure BIT reference gas and of the internal standard mixtures.

Internal standard	Mean δ^{15}N	σ	n	Internal standard mixture	Mean δ^{15}N	σ	n
BIT (100%)	−1.39	0.01	3	BIT (99.5%) + CO (0.5%)	−1.30	0.06	3
BIT (100%)	−1.34	0.08	3	BIT (99.5%) + CO (0.5%)	−1.29	0.03	2
BIT (100%)	−1.34	0.08	3				
BIT (100%)	−1.28	0.01	3				
BIT (100%)	−1.28	0.02	3	BIT (85%) + CO_2 (15%)	−1.32	0.06	3
BIT (100%)	−1.26	0.01	2	BIT (85%) + CO_2 (15%)	−1.47	0.01	3
BIT (Indiana)	−1.32	0.08	5	BIT (99%) + CO (0.5%) + CH_4 (0.5%)	−1.22	0.07	3
BIT (BGR)	−1.46	0.14	3	BIT (99%) + CO (0.5%) + CH_4 (0.5%)	−1.35	0.09	3

Notes: δ^{15}N values are reported in δ‰ vs. Air. σ = standard deviation; n = number of measurements on the same aliquot of gas.

in Figure 4a). Such a pressure, equivalent to an injection volume of 1.35 µl (around 60 nmol) of nitrogen and 55 nl (around 2.5 pmol) of ^{36}Ar, produces a signal-to-noise ratio close to 7.

4. δ^{15}N results

Table 2 shows the results obtained from five injections of pure BIT reference gas at various pressure levels together with the results of the internal standard mixtures. Reported isotope data represent the arithmetic means of at least duplicate analyses.

As can be seen, this method gives accurate results for both pure nitrogen and gas mixtures. The precision of the δ^{15}N data for both the reference gas and the mixtures is better than 0.15 ‰.

Reproducibility for the δ^{15}N values (1σ) is within ±0.1 ‰. It seems that the precision and the accuracy of measurements are influenced neither by the amount of the injected volume nor by the gas mixture.

5. Evaluation of air contamination

As previously argued, the δ^{15}N values can be affected by air contamination. The addition of an atmospheric component (either air or air saturated water) might be intrinsic of the gas emission or might occur during sample collection and storing, or during analytic operations.

Based on the assumption that ^{36}Ar content in crustal and mantle-derived gas is negligible with respect to ^{36}Ar concentration in the atmosphere, the simultaneous determination of δ^{15}N values, N_2 and ^{36}Ar contents provide the opportunity to accurately evaluate the degree of air contamination.

The atmospheric nitrogen component (N_{2atm}) was estimated as follows:

$$N_{2atm} = {}^{36}Ar_{meas} \times \left(\frac{N_2}{{}^{36}Ar}\right)_{atm}, \quad (1)$$

where $^{36}Ar_{meas}$ is the measured ^{36}Ar content and $(N_2/^{36}Ar)_{atm}$ is the $N/^{36}Ar$ volume ratio in the atmospheric component ($N_2/^{36}Ar = 2.46 \times 10^4$ in dry air and $N_2/^{36}Ar = 1.13 \times 10^4$ in ASW at 20 °C).

Therefore, we use the following equation to compute the relative excess of nitrogen (N_{2deep}) with respect to atmospheric contamination:

$$N_{2deep} = \left(1 - \frac{N_{2atm}}{N_{2meas}}\right) \times 100. \quad (2)$$

Finally, if we assume that the measured $\delta^{15}N$ values result from a simple binary mixture of an atmospheric (A) and a complementary non-atmospheric deep component ($D = 1 - A$), i.e.

$$\delta^{15}N_{obs} = A \times \delta^{15}N_{atm} + D \times \delta^{15}N_{deep}, \tag{3}$$

therefore, the $\delta^{15}N$ values of the non-atmospheric nitrogen ($\delta^{15}N_{deep}$) for all the samples were finally calculated by solving Equation (3) with respect to $\delta^{15}N_{deep}$ as follows:

$$\delta^{15}N_{deep} = \frac{\delta^{15}N_{obs}}{(1 - A)}. \tag{4}$$

6. Application to natural gas samples

More than 30 gas samples were collected from various sites including five active volcanic systems (Etna, Vulcano Island, Campi Flegrei, Pantelleria and Azores Islands) and three regions (Western Sicily-Italy, North Portugal and Greece) with natural gas emissions.

Gases were collected from a variety of types of gas emissions including high- and low-temperature fumaroles, boiling and bubbling pools, and mofettes. N_2-rich samples were collected by pumping the gas with a syringe into a 30 mL Pyrex flask with two gas-tight stopcocks. CO_2-rich samples were collected following the method proposed by Giggenbach and Gougel [18] in evacuated 250 ml glass flasks filled with 50 ml 6 N NaOH solution. Water vapour, carbon dioxide, as well as other acid gases (e.g. HCl, HF and S-species) condense into the liquid phase while 'non-condensable' species such as nitrogen and noble gases become enriched in headspaces.

In Table 3 are reported the location and the type of gas manifestations, the main chemical composition, the N_2 and ^{36}Ar concentrations, and the nitrogen isotope composition. Many of these gas manifestations are definitely CO_2-dominated while only four sites have relatively high N_2 contents in the range between 38.9% vol. (Psoroneria in Greece) and 98.2 % vol. (Segesta in Western Sicily).

A good agreement was obtained by comparing nitrogen concentration determined with the proposed GC-IRMS method and those later performed by using conventional GC-HWD techniques (Table 3 and Figure 5). The only slight differences between the data obtained from the two methods may be due to the fact that the analyses were performed on two different aliquots of gases from the same flask.

Data from the collected samples were plotted in the $\delta^{15}N$ vs. $N_2/^{36}Ar$ diagram together with the fields relative to MORB, atmosphere (AIR-ASW) and crustal sediments (Figure 6). It can be seen that the measured $\delta^{15}N$ data cover a wide range from -2.5 to $+6.7$ ‰. Gas from Vulcano Island and Campi Flegrei fumaroles are generally enriched in heavy N isotopes. The most negative nitrogen isotope values were measured in gas collected from boiling pools at S. Miguel (Azores Islands) with $\delta^{15}N$ values around -2 ‰.

The measured $N_2/^{36}Ar$ ratios range from 1.38×10^4 slightly higher than the ASW ratio at 20 °C up to 3.4×10^6, which is close to those reported by Sano *et al.* [5] for mantle-derived ($6 \pm 2 \times 10^6$) and for crustal fluids ($>6 \times 10^6$).

Once the N_2 and ^{36}Ar contents were determined, from Equation (1), we computed the percentage of air contamination. We assumed air ($N_2/^{36}Ar = 2.46 \times 10^4$) as the atmospheric component for high-T fumaroles and mofettes. The atmospheric gases were thought to be equilibrated with the liquid phase at the respective water temperature for bubbling gases and at boiling temperature for samples collected from low-temperature fumaroles and boiling pool.

In Table 4, the $N_2/^{36}Ar$ ratios in ASW are reported as a function of water temperature, computed on solubility data from Weiss [19].

Table 3. Description of sampling sites and analytical results on collected gas samples.

Sample	Type of manifestation	Date	Dominant gas phases	N_2[a]% GC-HWD	N_2[a]% GC-HWD	N_2[a]% GC-IRMS	^{36}Ar	$\delta^{15}N$	$N_2/^{36}Ar$	A	D	$\delta^{15}N_{deep}$
Vulcano Island (Italy)												
F 0	High-T fumarole	01/06/06	H_2O vap-CO_2	0.88	n.d.	88.4	3.0	4.6	2.91E+05	9.0	91.0	5.1
F 0		27/07/06		1.06	92.5	92.0	4.0	4.2	2.28E+05	10.9	89.1	4.7
F 0		16/11/06		3.09	n.d.	86.9	1.0	4.7	8.92E+05	3.0	97.0	4.8
F 0		17/01/07		2.01	94.5	91.6	6.6	3.8	1.38E+05	17.9	82.1	4.6
F 0		12/09/07		0.99	94.1	91.3	1.0	4.5	9.22E+05	2.7	97.3	4.6
F 0		13/05/08		n.d.	n.d.	75.8	2.2	4.5	3.48E+05	7.1	92.9	4.9
F 11	High-T fumarole	11/09/07	H_2O vap-CO_2	0.88	56.9	59.0	0.5	4.7	1.11E+06	2.2	97.8	4.8
F 11		19/09/06		0.87	43.0	51.3	2.9	4.5	1.80E+05	14.0	86.0	5.2
F 11		26/07/06		2.64	81.9	83.3	4.3	3.8	1.95E+05	12.7	87.3	4.4
F 11		16/11/06		2.21	61.8	58.3	0.8	4.6	6.97E+05	3.5	96.5	4.7
F 11	High-T fumarole	16/01/07	H_2O vap-CO_2	1.85	74.0	74.7	1.8	4.7	4.25E+05	5.9	94.1	5.0
F 5 AT	High-T fumarole	16/11/06	H_2O vap-CO_2	2.90	66.5	65.8	9.4	2.7	7.01E+04	35.2	64.8	4.2
F 5 AT		16/01/07		1.07	83.3	83.4	4.4	4.1	1.92E+05	12.9	87.1	4.7
F 5 AT		11/09/07		0.90	33.2	33.2	3.3	3.5	9.97E+04	24.8	75.2	4.7
F A	High-T fumarole	16/11/06	H_2O vap-CO_2	1.45	96.4	88.5	0.4	4.8	2.17E+06	1.2	98.8	4.9
F A		16/01/07		2.90	87.1	91.0	14.4	2.9	6.32E+04	39.1	60.9	4.8
F A		11/09/07		0.90	82.5	81.5	0.9	4.8	8.69E+05	2.8	97.2	4.9
F0	High-T fumarole	19/09/06	H_2O vap-CO_2	0.79	n.d.	90.3	3.3	4.4	2.72E+05	9.3	90.7	4.9
FI 1	High-T fumarole	11/09/07	H_2O vap-CO_2	1.15	81.7	83.0	1.4	4.5	6.07E+05	4.1	95.9	4.7
FI 2	High-T fumarole	11/09/07	H_2O vap-CO_2	n.d.	49.1	50.4	1.8	4.4	2.77E+05	8.9	91.1	4.9
FI 3	High-T fumarole	11/09/07	H_2O vap-CO_2	1.04	62.4	63.4	1.2	4.6	5.47E+05	4.5	95.5	4.8
FI 4	High-T fumarole	11/09/07	H_2O vap-CO_2	n.d.	82.9	83.0	0.9	4.8	8.95E+05	2.9	97.1	4.9
FI 5	Low-T fumarole (boiling T)	11/09/07	H_2O vap-CO_2	n.d.	60.0	60.2	0.9	4.8	6.80E+05	1.9	98.1	4.9
FB 1	Low-T fumarole (boiling T)	11/09/07	H_2O vap-CO_2	0.99	42.0	41.8	2.5	4.1	1.69E+05	7.8	92.2	4.5
FB 2	Low-T fumarole (boiling T)	11/09/07	H_2O vap-CO_2	0.87	98.2	94.6	1.4	4.6	6.82E+05	2.1	97.9	4.7
FC S	Low-T fumarole (boiling T)	13/05/08	H_2O vap-CO_2	n.d.	n.d.	91.7	2.9	4.8	3.21E+05	4.1	95.9	5.0
Azores Archipelago (Portugal)												
Furnas do Enxufre – Terceira	Low-T fumarole (boiling T)	13/02/08	H_2O vap-CO_2	0.47	23.9	24.4	14.5	−0.64	1.68E+04	76.0	24.0	−2.5
Furnas do Enxufre 2 – Terceira	Low-T fumarole (boiling T)	13/02/08	H_2O vap-CO_2	n.d	26.0	24.5	14.5	−0.7	1.69E+04	75.5	24.5	−2.9
Furnas do Enxufre – Terceira	Low-T fumarole (boiling T)	27/09/08	H_2O vap-CO_2	1.75	24.8	24.6	13.3	−0.3	1.85E+04	69.1	30.9	−0.8
Furna do Enxufre – Graciosa	Low-T fumarole (boiling T)	28/09/08	H_2O vap-CO_2	0.29	n.d.	80.9	43.3	−1.1	1.87E+04	68.6	31.4	−3.5
Furna do Enxufre – Graciosa	Boiling mud pool	28/09/08	CO_2	n.d.	n.d.	63.5	26.5	−1.1	2.39E+04	53.5	46.5	−2.3
Furna do Enxufre – Graciosa	Boiling mud pool	16/02/08	CO_2	0.28	72.4	65.6	27.5	−0.7	2.38E+04	53.7	46.3	−1.6

(*Continued*)

Table 3. Continued.

Sample	Type of manifestation	Date	Dominant gas phases	N_2[a]% GC-HWD	N_2[a]% GC-HWD	N_2[a]% GC-IRMS	^{36}Ar	$\delta^{15}N$	$N_2/^{36}Ar$	A	D	$\delta^{15}N_{deep}$
Caldeira Grande – S. Miguel	Boiling pool	19/02/08	H_2O vap-CO_2	0.28	51.4	41.3	23.1	−2.5	1.78E+04	71.8	28.2	−8.8
Caldeira Esguicho – S. Miguel	Boiling pool	19/02/08	H_2O vap-CO_2	0.21	49.6	46.1	26.1	−2.1	1.77E+04	72.3	27.7	−7.5
Caldeira da lagoa – S. Miguel	Boiling pool	19/02/08	H_2O vap-CO_2	0.27	86.8	79.3	51.4	−2.1	1.54E+04	83.0	17.0	−12.5
Caldeira Velha – S. Miguel	Boiling pool	20/02/08	H_2O vap-CO_2	0.34	71.9	63.5	42.9	−1.6	1.48E+04	86.4	13.6	−12.1
Northern Portugal												
Sandim	Bubbling gas ($T = 16°C$)	19/07/06	CO_2	n.d.	n.d.	76.1	34.0	1.0	2.24E+04	50.1	49.9	2.0
Messagaes	Bubbling gas ($T = 18°C$)	19/07/06	CO_2	n.d.	n.d.	92.8	44.3	0.3	2.10E+04	53.6	46.4	0.7
S. Pedro do Sul	Bubbling gas ($T = 62°C$)	19/07/06	N_2	94.3	–	94.3	45.6	0.5	2.07E+04	59.5	40.5	1.1
Melgaco AC2	Bubbling gas ($T = 18, 6°C$)	19/07/06	CO_2	n.d.	n.d.	86.6	42.0	0.8	2.06E+04	54.8	45.2	1.9
Melgaco AC1	Bubbling gas ($T = 20, 4°C$)	20/07/06	CO_2	n.d.	n.d.	90.2	45.7	0.7	1.97E+04	57.3	42.7	1.6
Chaves	Bubbling gas ($T = 67°C$)	20/07/06	CO_2	n.d.	n.d.	90.3	49.1	2.4	1.84E+04	67.2	32.8	7.3
Pantelleria Island (Italy)												
Gadir	Bubbling gas ($T = 53°C$)	01/03/06	CO_2	n.d.	n.d.	74.6	33.5	−1.1	2.23E+04	53.6	46.4	−2.5
Greece												
Sousaki grotta	Low-T fumarole (boiling T)	26/06/06	H_2O vap-CO_2	0.19	n.d.	69.2	10.1	4.7	6.86E+04	36.1	63.9	7.4
Psoroneria 2	Bubbling gas ($T = 40°C$)	27/03/08	CO_2-N_2	36.7		38.9	13.6	1.8	2.86E+04	40.9	59.1	3.1
C. Flegrei (Italy)												
BB	Low-T fumarole (boiling T)	31/01/07	H_2O vap-CO_2	n.d.	52.2	54.4	3.2	5.2	1.70E+05	14.6	85.4	6.1
BB		22/06/07		n.d.	58.4	54.8	6.0	4.4	9.18E+04	27.1	72.9	6.0
BG	Low-T fumarole ($T = 160°C$)	10/10/06	H_2O vap-CO_2	0.63	51.9	47.3	0.3	6.4	1.36E+06	1.8	98.2	6.6
BG		31/01/07		0.49	47.2	50.4	0.5	6.6	1.07E+06	2.3	97.7	6.7
BG		22/06/07		0.26	50.1	46.9	0.1	6.7	3.39E+06	0.7	99.3	6.8
BG		02/07/08		n.d.	n.d.	47.8	2.3	6.7	2.04E+05	12.1	87.9	7.7
BN	Low-T fumarole ($T = 130°C$)	10/10/06	H_2O vap-CO_2	0.42	52.6	49.7	0.4	6.5	1.27E+06	1.9	98.1	6.6
BN		31/01/07		0.98	47.5	49.3	0.5	6.6	1.07E+06	2.3	97.7	6.7
BN		22/06/07		0.22	48.6	47.2	0.5	6.6	8.58E+05	2.9	97.1	6.8
BN		02/07/08		n.d.	n.d.	49.5	2.2	6.6	2.26E+05	10.9	89.1	7.4
Fangaia	Boiling mud pool	10/10/06	CO_2	0.41	72.9	71.1	19.7	4.1	3.61E+04	29.6	70.4	5.8

Mt Etna (Italy)												
Naftia	Mofette	07/06/06	CO_2	0.49	39.2	37.0	6.6	−1.5	5.57E+04	44.3	55.7	−2.6
Naftia		06/07/06		0.46	37.8	36.6	5.5	−1.7	6.64E+04	37.2	62.8	−2.7
Naftia		05/10/06		0.49	49.1	46.1	7.6	−1.4	6.03E+04	40.9	59.1	−2.4
Naftia		12/10/06		0.48	47.4	47.0	7.2	−1.4	6.56E+04	37.6	62.4	−2.2
Naftia		18/10/06		0.49	49.0	44.8	6.6	−1.3	6.79E+04	36.4	63.6	−2.0
Naftia		24/10/06		0.50	47.9	47.2	8.2	−1.5	5.77E+04	42.8	57.2	−2.7
Naftia		08/11/06		0.47	n.d.	45.8	7.8	−1.4	5.84E+04	42.3	57.7	−2.4
Naftia		15/11/06		0.46	47.3	44.4	7.2	−1.6	6.19E+04	39.9	60.1	−2.6
Naftia		22/11/06		0.52	45.9	44.6	8.0	−1.5	5.57E+04	44.3	55.7	−2.7
Naftia		28/11/06		0.42	45.2	44.6	6.2	−1.6	7.19E+04	34.3	65.7	−2.4
Naftia		04/01/07		0.43	52.0	51.5	11.4	−1.4	4.53E+04	54.5	45.5	−3.1
Naftia		16/01/07		0.44	48.2	46.1	7.5	−1.5	6.13E+04	40.3	59.7	−2.4
Naftia		14/02/07		0.58	46.3	49.5	7.5	−1.4	6.57E+04	45.2	54.8	−2.6
Naftia		13/03/07		0.46	n.d.	46.5	6.0	−1.2	7.72E+04	32.0	68.0	−1.8
Naftia		22/11/07		0.48	44.2	44.6	5.3	−1.4	8.44E+04	29.4	70.6	−2.0
Naftia		13/03/08		0.42	52.4	50.8	6.6	−1.2	7.70E+04	45.8	54.2	−2.2
Stadio	Bubbling gas ($T = 20°C$)	18/10/06	CO_2-CH_4	0.18	3.0	2.4	1.1	−1.2	2.32E+04	49.0	51.0	−2.5
Stadio		24/10/06		0.12	8.8	7.8	3.8	−1.6	2.07E+04	54.7	45.3	−3.6
Stadio		15/11/06		0.19	3.2	2.7	1.5	−1.4	1.73E+04	65.4	34.6	−4.1
Stadio		22/11/06		0.13	2.9	3.1	1.6	−1.7	1.96E+04	58.1	41.9	−4.1
Western Sicily (Italy)												
Vuturo secco	Bubbling gas ($T = 30°C$)	14/09/06	N_2	66.3	–	65.1	23.9	0.3	2.73E+04	42.2	57.8	0.4
Segesta	Bubbling gas ($T = 45°C$)	14/09/06	N_2	94.5	–	95.3	37.2	0.5	2.56E+04	46.1	53.9	1.0
Air											0.0	2.47E+04
ASW (20°C)											0.0	1.13E+04
MORB											-5 ± 2 [5]	4÷8 E+06[a] [5]
Sediment											7±4 [5]	> 6.0E+06 [5]

Notes: $\delta^{15}N$ values are expressed in delta per mil vs. N_2–air; ^{36}Ar contents are expressed in ppm-vol. N_2 concentrations are expressed in % vol.; A and D express the relative nitrogen percentage of the atmospheric (A) and the complementary deep (D) end-member, respectively; $\delta^{15}N_{deep}$ are the $\delta^{15}N$ values corrected for air contamination (for more details, see text); MORB, mid-ocean Ridge basalt; n.d., not determined.

[a]Free gas.

[b]Residual gas in headspace (for more details, see text).

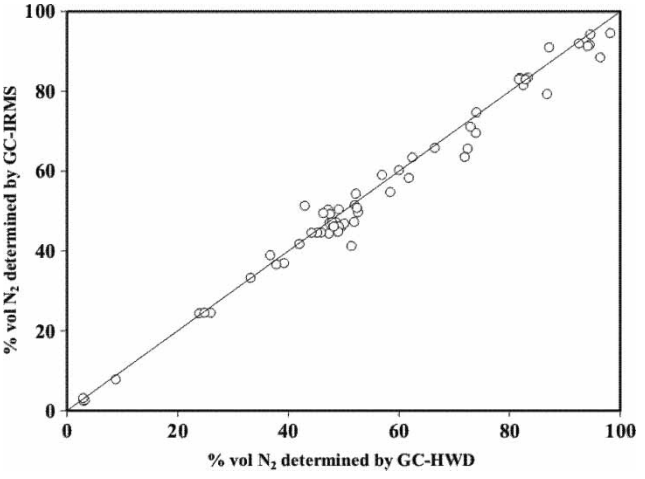

Figure 5. Data comparison between N_2 concentrations obtained with conventional GC-HWD techniques (x axis) and those carried out using the proposed method (y axis)

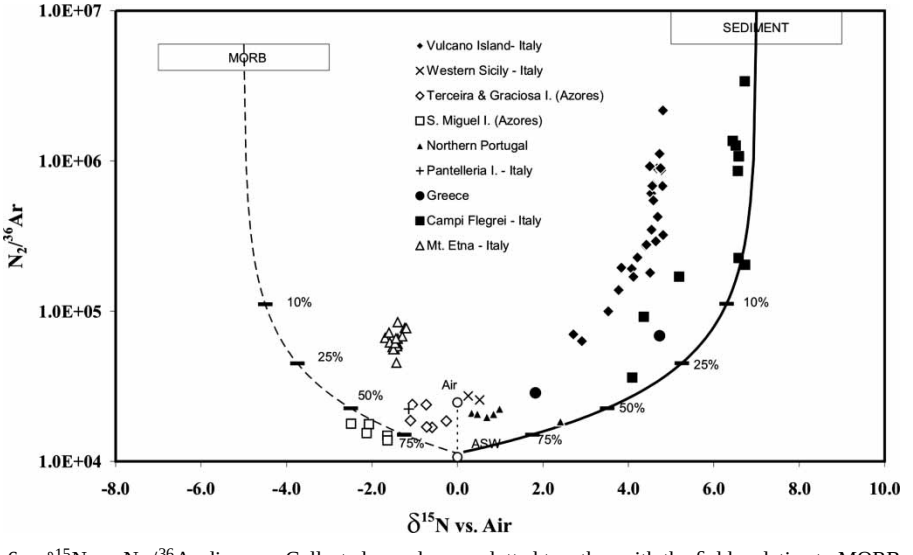

Figure 6. δ^{15}N vs. $N_2/^{36}$Ar diagram. Collected samples are plotted together with the fields relative to MORB, atmosphere (AIR/ASW at 20°C) and crustal sediments and two theoretical mixing curves between ASW (at 20°C) and average MORB composition (dotted line) and between ASW (at 20°C) and average sediment composition (solid line). Four relative percentages (10%, 25%, 50% and 75%) of the atmospheric component have been also highlighted.

The computed atmospheric nitrogen component is almost negligible in some fumarolic gas from Vulcano Island (Aeolian Archipelago) and C. Flegrei ($N_{2atm} = 0.7\,\%$ and $N_{2deep} = 99.3\,\%$), while it reaches about 86.4 % of the total nitrogen ($N_{2deep} = 13.6\,\%$) in the Caldeira Velha sample (São Miguel Island, Azores). Then, following Equation (4), the δ^{15}N values were corrected for air contamination, thus obtaining the nitrogen isotope composition of the complementary deep end-member ($\delta^{15}N_{deep}$).

Samples from Vulcano Island and C. Flegrei show $\delta^{15}N_{deep}$ values in the range from +5.5 to +7.7 ‰. These values indicate that in these fluids, nitrogen derives mainly from crustal materials. In fact, Aeolian Islands are part of an active volcanic arc originated from the subduction of oceanic and continental crust beneath the Eurasian plate [20]. According to Martelli *et al.* [21],

Table 4. Temperature dependence of nitrogen and ^{36}Ar solubility in water equilibrated with air.

T(°C)	N_2	$^{36}Ar *10^{-4}$	$N_2/^{36}Ar *10^4$
5	16.4	14.89	1.10
10	14.7	13.23	1.11
15	13.3	11.88	1.12
20	12.2	10.78	1.13
25	11.3	9.88	1.14
30	10.5	9.14	1.15
35	9.9	8.53	1.16
40	9.4	8.02	1.17
45	9.0	7.60	1.18
50	8.7	7.26	1.19
55	8.4	6.97	1.20
60	8.2	6.74	1.22
65	8.1	6.56	1.23
70	8.0	6.42	1.24
75	7.9	6.31	1.25
80	7.9	6.24	1.27
85	7.9	6.20	1.28
90	8.0	6.19	1.29
95	8.1	6.20	1.31

Notes: Data of N_2 and ^{36}Ar are expressed in cc STP gas per litre of pure water; ^{36}Ar solubility data were obtained from Ar solubility and $^{40}Ar/^{36}Ar = 295.5$ (air ratio) considering that no isotope fractionation occurs during dissolution in water; Solubility values (β) were computed from the following equation reported in Ozima and Podosek [17]:

$$\ln \beta = A_1 + A_2(100/T) + A_3 \ln(T/100) + S[B_1 + B_2(T/100) + B_3(T/100)^2],$$

where T is the temperature (K), S is salinity (in per mil). Coefficients (from [19]) as follows:

Ar : $A_1 = -55.6578$; $A_2 = 82.0262$; $A_3 = 22.5929$; $B_1 = -0.036267$; $B_2 = 0.016241$; $B_3 = -0.0020114$.

$\mathbf{N}_2$: $A_1 = -59.6274$; $A_2 = 85.7661$; $A_3 = 24.3696$; $B_1 = -0.051580$; $B_2 = 0.026329$; $B_3 = -0.0037257$.

the mantle beneath the C. Flegrei region has metasomatised by the addition of crustal fluids from the subducted plate.

Previous investigations carried out on the Azores Islands allowed us to recognise at least three different source components: a mantle plume, a MORB-source mantle deriving from the adjacent MAR segment and an enriched (crustal) component most strongly evident in the lavas of Sao Miguel. The δ^{15}N data from the Azores Islands seem to indicate that a genetic difference at the scale of the archipelago also exists in nitrogen isotopes' signature. Fluids collected from São Miguel Island show the more depleted $\delta^{15}N_{deep}$ values (from -7.5 to -12.5 ‰) resembling MORBs values. This insight indicates that, in this magmatic system, there is no evidence of any crustal source as already suggested considering other geochemical tracers [22,23].

δ^{15}N values from Graciosa and Terceira Islands between -3.5 ‰ and -0.8 ‰ seem to support the hypothesis that fluids degassing from a mantle plume, probably located beneath the central group islands, interact with the overlying upper mantle as suggested by primordial Neon isotopes [24] as well as by helium isotope data slightly above those typical for MORBs [25].

All the other samples show intermediate $\delta^{15}N_{deep}$ values between MORBs and sediments. Gases collected from these sites probably reflect different degrees of interaction between mantle- and crustal-derived fluids, consistent with the $^3He/^4He$ ratios [26–29].

7. Conclusions

A new CF-GC/IRMS method to analyse the nitrogen isotope composition of molecular nitrogen (N_2) in gas samples was developed. The proposed method tested injecting samples with N_2 volume

in the range between 0.05 and 2 μmol, provided reliable δ^{15}N values with accuracy better than 0.15‰. Reproducibility for the δ^{15}N values (1σ) is within ±0.1‰.

The method was tested on magmatic and hydrothermal gases as well as on natural gas samples collected from various sites related to several different geological frameworks.

The used instrument was also set to determine in the same run the concentrations of N_2 and ^{36}Ar. Therefore, on the basis of the simultaneously obtained $N_2/^{36}$Ar ratios, it is possible to accurately evaluate the degree of atmospheric contamination. Finally, by using simple mixing equations, the air-corrected $\delta^{15}N_{deep}$ values were computed.

The $\delta^{15}N_{deep}$ values, collected from a variety of types of gas emissions, cover a wide range from −12.5‰ to +7.7‰, and agree well with the respective geodynamic context. The obtained data confirm that the nitrogen isotope ratios in magmatic and hydrothermal gases are good geochemical tracers of volatiles' source.

Acknowledgements

The authors are indebted to E. Faber (BGR, Hannover, Germany) and A. Schimmelman (Indiana University, USA) for helping with nitrogen isotope analyses. Our colleagues M. Martelli, A. Rizzo, F. Salerno and M. Tantillo (INGV-Palermo, Italy) are also thanked for their technical support during chemical gas analyses. Thanks are also due to two anonymous reviewers for their extremely helpful and constructive suggestions. This work was partially funded by FCT in the framework of the project INOGAZ (PTDC/CTE-GIN/68851/2006).

References

[1] B. Marty and F. Humbert, Nitrogen and Argon Isotopes in Oceanic Basalts, *Earth Plan. Sci. Lett.* **152**, 101 (1997).
[2] Y. Sano, N. Takahata, Y. Nishio, T.P. Fischer, and S.N. Williams, Volcanic Flux of Nitrogen from the Earth, *Chem. Geol.* **171**, 263 (2001).
[3] S. Inguaggiato, Y. Taran, F. Grassa, G. Capasso, R. Favara, N. Varley, and E. Faber, Nitrogen Isotopes in Thermal Fluids of a Forearc Region (Jalisco Block, Mexico): Evidence for Heavy Nitrogen from Continental Crust. *Geochem. Geophys. Geosyst.* **5**, Q12003 (2004).
[4] B. Marty and N. Dauphas The Nitrogen Record of Crust–Mantle Interaction and Mantle Convection from Archean to Present, *Earth Plan. Sci. Lett.* **206**, 397 (2003).
[5] Y. Sano, N. Takahata, Y. Nishio, and B. Marty, Nitrogen Recycling in Subduction Zones, *Geophys. Res. Lett.* **25**, 2289 (1998).
[6] M.M. Zimmer, T.P. Fischer, D.R. Hilton, G.E. Alvarado, Z.D. Sharp, and J.A. Walker, Nitrogen Systematics and Gas Fluxes of Subduction Zones: Insights from Costa Rica Arc Volatiles, *Geochem. Geophys. Geosyst.* **5**, Q05J11 (2004).
[7] L.E. Clor, T.P. Fischer, D.R. Hilton, Z.D. Sharp, and U. Hartono, Volatile and N Isotope Chemistry of the Molucca Sea Collision Zone: Tracing Source Components Along the Sangihe Arc, Indonesia, *Geochem. Geophys. Geosyst.* **6**, Q03J14 (2005).
[8] T.P. Fischer, N.C. Sturchio, J. Stix, G. Arehart, D. Counce, and S.N. Williams, The Chemical and Isotopic Composition of Fumarolic Gases and Spring Discharges from Galeras Volcano, Colombia, *J. Volcanol. Geotherm. Res.* **77**, 229 (1997).
[9] T.P. Fischer, N. Takahata, Y. Sano, H. Sumino, and D.H. Hilton, Nitrogen Isotopes of the Mantle: Insights from Mineral Separates, *Geophys. Res. Lett.* **32**, L11305 (2005).
[10] I.N. Tolstikhin and B. Marty, The Evolution of Terrestrial Volatiles: A View from Helium, Neon, Argon and Nitrogen Isotope Modeling, *Chem. Geol.* **147**, 27 (1998).
[11] T. Matsumoto, D. Pinti, J. Matsuda, and S. Umino, Recycled Noble Gas and Nitrogen in the Subcontinental Lithospheric Mantle: Implications from N–He–Ar in Fluid Inclusions of SE Australian Xenoliths, *Geochem. J.* **36**, 209 (2002).
[12] R.K. Mohapatra, D. Harrison, U. Ott, J.D. Gilmour, and M. Trieloff, Noble Gas and Nitrogen Isotopic Components in Oceanic Island Basalts, *Chem. Geol.* **266**, 29 (2009).
[13] C. Ballentine and B. Sherwood Lollar, Regional Groundwater Focusing of Nitrogen and Noble Gases into the Hugoton-Panhandle Giant Gas Field, USA, *Geochim. Cosmochim. Acta* **66**, 2483 (2002).
[14] K.A. Farley, R.J. Poreda and T.C. Onstott, Noble Gases in Deformed Xenoliths from an Ocean Island: Characterisation of a Metasomatic Fluid, in *Noble Gas Geochemistry and Cosmochemistry*, edited by J. Matsuda (Terra Scientific, Tokyo, 1994), pp. 159–178.
[15] P.G. Burnard, D.W. Graham, and G. Turner, Vesicle-specific Noble Gas Analyses of 'Popping Rock': Implication for Primordial Noble Gases, *Earth Sci.* **276**, 568 (1997).

[16] A.O. Nier, A Redetermination of the Relative Abundances of the Isotopes of Carbon, Nitrogen, Oxygen, Argon and Potassium, *Phys. Rev.* **77**, 789 (1950).
[17] M. Ozima, and F.A. Podosek, *Noble Gas Geochemistry* (Cambridge University Press, Cambrige, 1983).
[18] W.F. Giggenbach and R.L. Gougel, *Methods for the Collection and Analyses of Geothermal and Volcanic Water and Gas Samples* (DSIR, Chemical Division, Petone, New Zealand, 1989).
[19] R.F. Weiss, The Solubility of Nitrogen, Oxygen and Argon in Water and Seawater, *Deep Sea Res.* **17**, 721 (1970).
[20] F. Barberi, F. Innocenti, G. Ferrara, J. Keller, and L. Villari, Evolution of Aeolian Arc Volcanism (Southern Tyrrhenian Sea), *Earth Planet. Sci. Lett.* **21**, 269 (1974).
[21] M. Martelli, P.M. Nuccio, F.M. Stuart, R. Burgess, R.M. Ellam, and F. Italiano, Helium Strontium Isotopic Constrains on Mantle Evolution Beneath the Roman Comagmatic Province, Italy. *Earth Planet. Sci. Lett.* **224**, 295 (2004).
[22] C. Beier, A. Stracke, and K.M. Haase, The Peculiar Geochemical Signatures of (Azores) Lavas: Metasomatised or Recycled Mantle Sources? *Earth Plan. Sci. Lett.* **259**, 186 (2007).
[23] T. Elliott, J. Blichert-Toft, A. Heumann, G. Koetsier, and V. Forjaz, The Origin of Enriched Mantle Beneath São Miguel, Azores, *Geochim. Cosmochim. Acta* **71**, 219 (2007).
[24] P. Madureira, M. Moreira, J. Mata, and C.J. Allègre, Primitive Neon Isotopes in Terceira Island (Azores Archipelago), *Earth Plan. Sci. Lett.* **233**, 429 (2005).
[25] M. Moreira, R. Doucelance, B. Dupre, M. Kurz, and C.J. Allègre, Helium and Lead Isotope Geochemistry in the Azores Archipelago, *Earth Plan. Sci. Lett.* **169**, 189 (1999).
[26] P.M. Carreira, J.M. Marques, M.R. Carvalho, G. Capasso, and F. Grassa, Mantle-Derived Carbon in Hercynian Granites. Stable Isotopes Signatures and C/He Associations in the Thermomineral Waters, N-Portugal, *J. Volcanol. Geotherm. Res.* **189**, 49 (2010).
[27] A. Caracausi, R. Favara, F. Italiano, P.M. Nuccio, A. Paonita, and A. Rizzo, Active Geodynamics of the Central Mediterranean Sea: Tensional Tectonic Evidences in Western Sicily from Mantle-Derived Helium, *Geophys. Res. Lett.* **32**, L04312 (2005); doi:10.1029/2004GL021608.
[28] P. Allard, P. Jean-Baptiste, W. D'Alessandro, F. Parello, B. Parisi, and C. Flehoc, Mantle-Derived Helium and Carbon in Groundwaters and Gases of Mount Etna, Italy, *Earth Plan. Sci. Lett.* **148**, 501 (1997).
[29] W. D'Alessandro, L. Brusca, K. Kyriakopoulos, G. Michas, and G. Papadakis, Methana, the Westernmost Active Volcanic System of the South Aegean Arc (Greece): Insight from Fluids Geochemistry, *J. Volcanol. Geotherm. Res.* **178**, 818 (2008).